

Persistent inflammation alters the function of the endogenous brain stem cell compartment

Stefano Pluchino,^{1,2} Luca Muzio,^{1,2} Jaime Imitola,³ Michela Deleidi,^{1,2} Clara Alfaro-Cervello,⁴ Giuliana Salani,^{1,2} Cristina Porcheri,^{1,2} Elena Brambilla,^{1,2} Francesca Cavasinni,^{1,2} Andrea Bergamaschi,^{1,2} Jose Manuel Garcia-Verdugo,^{4,5} Giancarlo Comi,² Samia J. Khoury^{3,*} and Gianvito Martino^{1,2,*}

¹Neuroimmunology Unit, DIBIT, ²Institute of Experimental Neurology (INSPE), San Raffaele Scientific Institute, 20132 Milan, Italy, ³Center for Neurologic Diseases and Partners Multiple Sclerosis Center, Department of Neurology, Brigham and Women's Hospital, Harvard Medical School, Boston, MA 02115, USA, ⁴Department Comparative Neurobiology, Instituto Cavanilles, University of Valencia, 46980 Valencia and ⁵Department of Cellular Therapy, Centro de Investigación Príncipe Felipe, 46013 Valencia, Spain

*These authors contributed equally to this work.

Correspondence to: Gianvito Martino, MD, Neuroimmunology Unit – DIBIT and INSPE, San Raffaele Scientific Institute, Via Olgettina 58, 20132 Milano, Italy
E-mail: martino.gianvito@hsr.it

Endogenous neural stem/precursor cells (NPCs) are considered a functional reservoir for promoting tissue homeostasis and repair after injury, therefore regenerative strategies that mobilize these cells have recently been proposed. Despite evidence of increased neurogenesis upon acute inflammatory insults (e.g. ischaemic stroke), the plasticity of the endogenous brain stem cell compartment in chronic CNS inflammatory disorders remains poorly characterized. Here we show that persistent brain inflammation, induced by immune cells targeting myelin, extensively alters the proliferative and migratory properties of subventricular zone (SVZ)-resident NPCs *in vivo* leading to significant accumulation of non-migratory neuroblasts within the SVZ germinal niche. In parallel, we demonstrate a quantitative reduction of the putative brain stem cells proliferation in the SVZ during persistent brain inflammation, which is completely reversed after *in vitro* culture of the isolated NPCs. Together, these data indicate that the inflamed brain microenvironment sustains a non cell-autonomous dysfunction of the endogenous CNS stem cell compartment and challenge the potential efficacy of proposed therapies aimed at mobilizing endogenous precursors in chronic inflammatory brain disorders.

Keywords: neurogenesis; neural stem cells; inflammation; experimental autoimmune encephalomyelitis; multiple sclerosis

Abbreviations: BrdU = 5'-bromo-2'-deoxyuridine; CFA = complete Freund's adjuvant; dpi = days post-immunization; EAE = experimental autoimmune encephalomyelitis; EGF = epidermal growth factor; EM = electron microscopy; FGF-II = fibroblast growth factor; GFAP = glial-fibrillary acidic protein; HC = healthy control; IddU = 5'-iodo-2'-deoxyuridine; IFN- γ = interferon- γ ; IL-1 β = interleukin-1 β ; L.I. = labelling index; MOG = myelin oligodendrocyte glycoprotein; NCFCA = Neural Colony Forming Cell Assay; NS-A = Neurosphere Assay; NPC = neural stem/precursor cells; OB = olfactory bulb; PDGF = platelet-derived growth factor; PSA-NCAM = polysialylated form of neural cell adhesion molecule; RMS = rostral migratory stream; SVZ = subventricular zone; TLDA = TaqMan[®] Low-Density Array; TNF- α = tumour necrosis factor- α .

Received March 10, 2008. Revised July 27, 2008. Accepted July 31, 2008. Advance Access publication August 30, 2008

Introduction

Multipotent neural stem/precursor cells (NPCs), supporting self-renewal and differentiation, reside within specialized compartments or niches in the adult mammalian CNS (Doetsch, 2003). One of the best characterized niches is the subventricular zone (SVZ), a layer of cells lying immediately

under the ependymal lining of the lateral ventricles (Martino and Pluchino, 2006). The SVZ has great potential for neurogenesis, both in rodents and humans, and contains three major cell types. The CNS stem cells (type B cells) that display an astrocyte-like phenotype express the glial-fibrillary acidic protein (GFAP) and give rise to intermediate transit

amplifying progenitors (type C cells), which lose the GFAP immunoreactivity and acquire the expression of the distal-less homeobox (Dlx)-2. These type C cells can, in turn, differentiate into neuroblasts (type A cells) that express the polysialylated form of neural cell adhesion molecule (PSA-NCAM) in addition to doublecortin, and migrate to the olfactory bulb (OB). The cell lineage differentiation pathway proceeds from type B, through type C, to type A cells, with the type B cell believed to be the self-renewing CNS stem cell (Alvarez-Buylla and Garcia-Verdugo, 2002).

The relative contribution of the different cell types of the SVZ germinal niche to tissue repair upon CNS injury is still matter of debate. While it is clear that there is a boost of neurogenesis following acute inflammatory insults, such as ischaemic stroke (Zhang *et al.*, 2004; Jin *et al.*, 2006), there is contradictory evidence on the response of the endogenous brain stem cell compartment to chronic CNS inflammation leading to neurodegeneration. CNS germinal niches may be impaired following either cranial irradiation or lipopolysaccharide-mediated acute inflammation (Martino and Pluchino, 2006). Previous studies in mice with experimental autoimmune encephalomyelitis (EAE) have reported transient increase in proliferation of PSA-NCAM⁺ and NG2⁺ proteoglycan cells in the corpus callosum, inferred as evidence of enhanced proliferation of stem and precursor cells in the SVZ (Calza *et al.*, 1998; Picard-Riera *et al.*, 2002; Nait-Oumesmar *et al.*, 2007). However, none of these studies has directly addressed the changes in the specific cell types in the SVZ during EAE.

Here we have studied the effects chronic inflammatory demyelination on the SVZ germinal niche using EAE, a mouse model of multiple sclerosis (Pluchino *et al.*, 2003). This model is very useful for studying the impact of chronic inflammation on the SVZ because in the C57BL/6 mouse strain the autoimmune reaction in the brain occurs as a consequence of the subcutaneous immunization with the myelin oligodendrocyte glycoprotein (MOG) (peptide 35–55) that targets the rostral and periventricular forebrain regions. (Brown and Sawchenko, 2007; Politi *et al.*, 2007).

Materials and Methods

EAE induction

Chronic-progressive EAE was induced in 6- to 8-week-old C57BL/6 female mice, as described (Pluchino *et al.*, 2003; Amadio *et al.*, 2006). For targeted EAE, MOG 35-55-immunized mice [20 days post immunization (dpi)] and healthy controls (HC) were stereotactically injected in the brain with 230 ng TNF- α and 250 ng IFN- γ (BD Biosciences, Franklin Lakes, NJ, USA) dissolved in a total volume of 2 μ l of sterile saline. Further information is provided in the Supplementary data.

In vivo analysis of cell cycle length and growth fraction

In order to label the entire population of fast proliferating SVZ cells, mice were intraperitoneally injected with 5'-iodo-2'-deoxyuridine

(IdU, the first injection was done at the concentration of 100 mg/kg in 0.007 N NaOH in 0.9% saline, while the following injections were done 70 mg/kg in 0.007 N NaOH in 0.9% saline) every 2 h for a total of 14 h, as described (Morshead and van der Kooy, 1992). Further information is provided in the Supplementary data.

In vivo analysis of slowly-dividing neural stem cells

In order to label the slowly dividing relatively quiescent SVZ putative neural stem cells, EAE mice received intraperitoneal 5'-bromo-2'-deoxyuridine (BrdU, 70 mg/kg in 0.007 N NaOH in 0.9% saline) every 8 h for a total of 6 consecutive days starting at either 13 or 30 dpi, as described (Morshead *et al.*, 1998). A washout period of 40 days was then chased before sacrifice. At sacrifice, brains were removed and fixed as described and serial 10 μ m coronal cryosections were generated and stained with rat anti-BrdU (clone ICR1; Abcam, Cambridge, UK) and rabbit anti-GFAP (DAKO) antibodies. BrdU⁺/GFAP⁺ cells were scored in a region ranging from bregma +1.2 to bregma +0 throughout the entire SVZ. One section every 70 μ m was analysed with 40 \times Leica Confocal (SP2) objectives. Double-labelled cells were confirmed by computer-aided three-dimensional reconstruction.

Retroviral injections for in vivo studies

Mice ($n=3$ per group) were anesthetized with 2,2,2-tribromoethanol (10 mg/ml; 1/27 of body weight) and the head was placed in a stereotactic injection apparatus (David Kopf Instruments, Tujunga, CA, USA). As previously described (Carleton *et al.*, 2003; Menn *et al.*, 2006), a replication-defective retrovirus expressing the GFP under the CMV promoter (rkat 43.2) (Montini *et al.*, 2006) was injected within the right lateral ventricle at the following coordinates: A. +0; L. +0.8 and D. -2.4. Further information is provided in the Supplementary data.

In situ hybridization

In situ hybridization was performed according to standard methods, as described (Mallamaci *et al.*, 2000). Further information is provided in the Supplementary data.

Immunofluorescence and immunohistochemistry

At the time of sacrifice, mice were anesthetized and transcardially perfused with PBS followed by 4% paraformaldehyde. The brains were removed and processed for light and electron microscopy (EM), as described (Pluchino *et al.*, 2003). Antigen retrieval, when appropriate, was performed as previously indicated (Muzio *et al.*, 2005), while endogenous peroxidase blocking reaction was obtained by incubating sections 20 min in methanol/H₂O₂ 3% solution. Further information is provided in the Supplementary data.

EM

Transmitted EM was performed as described previously (Doetsch *et al.*, 1997). Further information is provided in the Supplementary data.

Primary neural stem/precursor cell cultures

Neural stem cell cultures were established from the lateral ventricular walls of C57BL/6 6- to 8-week-old female mice, as described (Reynolds and Weiss, 1992). To analyse cell proliferation, primary cells isolated as above were plated at 8000 cells/cm² in

neurosphere growth medium (DMEM/F12 containing 2 mM L-glutamine, 0.6% glucose, 0.1 mg/ml apo-transferrin, 0.025 mg/ml insulin, 9.6 µg/ml putrescin, 6.3 ng/ml progesterone, 5.2 ng/ml Na selenite, 2 µg/ml heparin) supplemented with epidermal growth factor (EGF) (20 ng/ml) and fibroblast growth factor (FGF-II) (10 ng/ml), and spheres were collected after 3–5 days, as described (Politi *et al.*, 2007). Further information is provided in the Supplementary data.

In vitro Neurosphere Formation Assay (NS-A)

Primary cells isolated as above from HC, complete Freund's adjuvant (CFA) and EAE immunized mice ($n=3$ each) and plated in 24-well (0.5 ml/well) uncoated plates (Corning, Corning, NY, USA) at a density of 8000 cells/cm² in growth medium, as described (Politi *et al.*, 2007). Further information is provided in the Supplementary data.

Neural Colony Forming Cell Assay (NCFCA)

Primary cells isolated as above from HC, CFA and EAE immunized mice ($n=6$ each) were plated using the mouse NeuroCult neural colony-forming cell assay kit (StemCell Technologies, Vancouver, BC, Canada) as per the manufacturer's instructions, at a density of 6.5×10^5 cells per 35 mm cell culture dish with 2 mm grid (Nunc, Rochester, NY, USA), as described. Further information is provided in the Supplementary data.

Immunocytochemistry

Fixed cells were rinsed with PBS and incubated for 90 min at 37°C in PBS containing 10% normal goat serum (NGS), 0.3% Triton X-100, and appropriate primary antibodies or antisera, as described. Further information is provided in the Supplementary data.

Gene expression analysis

Two 96b Format TaqMan[®] Low-Density-based Array (TLDA) (167 different genes and 3 house keeping), for gene expression, were performed onto the SVZ tissue freshly derived from both EAE mice and HC. At due time points, SVZ tissue samples ($n=6$ mice per group) were homogenized in 1 ml of QIAzol Lysis Reagent (Qiagen, Valencia, CA, USA, #79306) using a rotor-stator homogenizer. Total RNA was isolated from homogenized tissue samples using RNeasy Lipid Tissue Kit (Qiagen, #74804) including Dnase digestion. At the end, RNA samples were redissolved in 30 µl of RNase-free water and their concentrations were determined spectrophotometrically by A₂₆₀ (Nanodrop-ND 1000, Nanodrop, Wilmington, DE, USA). Further information is provided in the Supplementary data.

Sample preparation for laser-capture microdissection

At sacrifice, mice ($n \geq 4$ per group) were deeply anesthetized via an intraperitoneal injection of chloralium hydrate 8% and then were rapidly perfused transcardially with RNase-free 0.9% saline containing 10 U/ml of heparin. Brains were removed from the skulls and then OCT embedded and rapidly frozen by immersion in liquid nitrogen. Brains were stored at -80°C . Laser microdissection was performed using a Leica AS LMD instrument (Leica Microsystems, Milan, Italy). Further information is provided in the Supplementary data.

Flow cytometric and nuclear DNA analysis

Cells were plated at 8000 cells/cm² in growth medium with or without either Th1 [500 IU/ml recombinant mouse IFN- γ

(BD Biosciences), 200 UI/ml recombinant mouse TNF- α (Pepro Tech Inc., Rocky Hill, NJ, USA), 100 UI/ml recombinant mouse IL-1 β (Euroclone, Sizzano, Italy)] or Th2 [10 ng/ml recombinant murine IL-4 (R&D, Minneapolis, MN, USA), 10 ng/ml recombinant mouse IL-5 (R&D), 10 ng/ml recombinant mouse IL-13 (R&D)] cytokine mixes. After 48 h, cells were collected, mechanically dissociated and washed in PBS three times. For nuclear DNA content analysis, cells were then re-suspended in 81% PBS 1 \times , 1% ND P-40, 10% Propidium Iodide (PI), 8% RNase (Ribonuclease A 300 Kuntz Units) solution. Nuclear DNA content was analysed, as described (Chew *et al.*, 2005), and data collection was gated utilizing forward light scatter and side light scatter to exclude cell debris and aggregates. Growing fractions of both HC and cytokine-conditioned NPCs were also determined by the expression of the Ki67 antigen, which is expressed exclusively in proliferating cells during the late G1, S, G2 or M phase of the cell cycle. Following permeabilization with ice-cold 70% ethanol, cells were incubated with fluorescein isothiocyanate (FITC)-conjugated anti-Ki67 antibody (BD PharMingen, Franklin Lakes, NJ, USA). The PI fluorescence was measured on a linear scale using a FACS Cyan flow cytometer (Dako, Glostrup, Denmark), while the Ki67 staining was analysed using a BD FACSCanto II flow cytometer. All data were acquired and analysed using FCS 3 software (Becton Dickinson, Franklin Lakes, NJ, USA). At least 2×10^4 events/sample were analysed.

Statistical analysis

Data were compared using the Student's *t*-test for paired or unpaired data or the Mann–Whitney U-test for non-parametric data.

Results

Impaired proliferation of adult SVZ-resident NPCs

We first studied the influence of chronic CNS inflammation on the proliferation kinetics and fate of mitotically active progenitor cells (type C, B and A cells) in the SVZ of EAE and HC mice. The mouse model we adopted is highly suitable to study the interactions between inflammation and SVZ-resident NPCs as one third of the inflammatory infiltrates in the anterior forebrain at the peak of inflammation are specifically found within the ventral and dorsal SVZ. Six EAE mice were sacrificed at 30 dpi and forebrain inflammatory lesions were quantified. A total of 89 lesions (14, eight per mouse) were enumerated. Total 30/89 (33.7%) were classified as intraparenchymal lesions, 26/89 (29.2%) as SVZ lesions and 33/89 (37%) as leptomeningeal lesions (mean number per area: intraparenchymal = 5.0 ± 1.85 ; SVZ = 4.3 ± 0.85 ; leptomeningeal = 5.5 ± 1.54) (Supplementary Fig. 1). To study the cell cycle length and the growth fraction with the S-phase cumulative labelling technique, mice were intraperitoneally injected with saturating doses of IddU (Morshead and van der Kooy, 1992; Takahashi *et al.*, 1992). IddU⁺ cells were counted within the dorso- and ventro-lateral SVZ in a telencephalic region ranging from bregma +1.2 to bregma +0.

To study the rapidly dividing transit-amplifying progenitor cells (type C cells) we used short-term IddU labelling

Table 1 Cell cycle analysis of rapidly-dividing (type C) progenitor cells in the SVZ of EAE and HC mice

Mice ^a	No.	T_c ^b	GF ^c	r^{2d}	P-value
HC (6 weeks old)	27	12.2	27.2 ± 0.004	0.94	NA
HC (18 weeks old)	6	13.0	24.0 ± 0.4	0.89	NS**
CFA (6 weeks old)	8	12.2	26.9 ± 0.7	0.93	NS**
EAE 20 dpi	15	12.1	20.0 ± 2.1	0.89	0.002 [†]
EAE 30 dpi	15	12.9	19.1 ± 1.2	0.86	0.001 [†]
EAE 60 dpi	12	11.9	27.0 ± 1	0.86	NS [†]
EAE 90 dpi	8	12.3	24.7 ± 0.79	0.89	NS*

NA = not applicable; NS = not significant.

^aSix-weeks-old-mice have been immunized for EAE.

^bData are expressed as hours. T_c is the length of the entire cell cycle.

^cData are expressed as mean percentage of IddU⁺ cells (±SD) over total cell counts. GF represents the labelling time sufficient to label 100% of proliferating cells.

^dRegression analysis between the labelling index and the hours elapsed from the first IddU injection.

** versus HC 6 weeks old; [†] versus CFA; * versus HC 18 weeks old (all calculated using Student 't-test).

protocols (see Supplementary data). We did not find any significant difference in the cell cycle length (T_c) in the SVZ of EAE versus HC mice (Table 1). On the other hand, the GF of EAE mice at 20 and 30 dpi was significantly lower compared with HC (both $P \leq 0.05$), though a return toward baseline values was observed between 60 and 90 dpi (Table 1). Accordingly, a significant reduction in the absolute numbers of M-phase-confined phosphorylated histone H3 (pH3)⁺ SVZ cells was observed in EAE mice at 20, 30 and 60 dpi (Figure 1A) when compared with HC (all $P \leq 0.05$). Again, a return toward baseline values in the numbers of pH3⁺ cells was observed in EAE at 90 dpi (data not shown). Finally, few—if any—IddU⁺/Iba1⁺ and/or CD45⁺/Ki67⁺ cells were found within the SVZ of EAE mice (Figure 1B–E), thus suggesting that the proliferation of either local microglial cells or CNS-infiltrating blood-derived leucocytes did not contribute significantly to the total GF quantified within the dorso-lateral SVZ. Apoptosis of neural cells could not account for the observed decreased GF, as no difference in the number of caspase-3⁺ SVZ cells was found between EAE mice and HC (data not shown).

These data suggest that chronic CNS inflammation leads to a significant reduction of the GF—but not of the T_c —of SVZ-resident transit amplifying neural progenitors (type C cells), whose proliferation defect tends to recover as early as inflammation fades out.

To study the slowly dividing relatively quiescent putative CNS stem cells (type B cells), a long-term retention analysis (upon BrdU labelling) was performed (Morshead *et al.*, 1998). Label-retaining putative CNS stem cells of the adult SVZ (type B cells) share some key features with both radial glia as well as parenchymal astrocytes—including immunoreactivity for GFAP (Doetsch *et al.*, 1999). As unambiguous identification of these cells *in vivo* is difficult with conventional immuno detection techniques—due to the unavailability of exclusive molecular markers—CNS stem cells are defined by a combination of morphological, biological and molecular criteria as true glial cells, akin to astroglia (Pinto and Gotz, 2007). While no difference of label-retaining

SVZ cell was found at 13 dpi, a significant decrease in BrdU-retaining GFAP⁺ SVZ cells was observed in EAE mice at 30 dpi compared with HC ($P \leq 0.001$) (Fig. 1F). We also, performed *in situ* hybridization for the platelet-derived growth factor (PDGF) receptor α , a molecular marker which has been shown to be expressed by both relatively quiescent oligodendrocytes precursor cells (OPCs) of the rodent optic nerve and spinal cord (Raff *et al.*, 1983a, b) as well as by up to 80% of type B cells of the adult SVZ (Jackson *et al.*, 2006; Menn *et al.*, 2006). Consistent with the long-term retention analysis, substantial reduction of the SVZ cells expressing the mRNA for *PDGF α* was observed in EAE at 20 dpi, compared with HC ($P \leq 0.05$) (Fig. 1G).

Therefore, also a decrease of slowly dividing SVZ putative stem cells (type B cells) is observed at the peak of the inflammatory phase of EAE.

Altered temporal and spatial relationships between cells in the SVZ niche

To better characterize the morphological features of the different SVZ cell types suffering functional derangement in EAE, we performed light and EM analyses on transverse sections of the ventricular lateral wall of the anterior horn of the SVZ. Sections were obtained from both HC as well as EAE mice at 10, 20, 30 and 60 dpi and distinct SVZ cell types identified and scored according to established ultrastructural criteria (Doetsch *et al.*, 1997).

We did not observe any alteration of the morphological characteristics of each of the different cell types—such as increased smooth or rough endoplasmic reticula, or accumulation of mitochondria or lysosomes—in EAE mice compared with HC at each of the time points analysed. However, significant differences in cell distribution and organization were observed. Both semithin section analysis (Fig. 2A) as well as EM showed accumulation of type A progenitor cells and decrease of both type C and type B cells abutting the ventricle—probably activated type B cells—below the ependymal ribbon in EAE mice at 10–30 dpi (Fig. 2A, B and E).

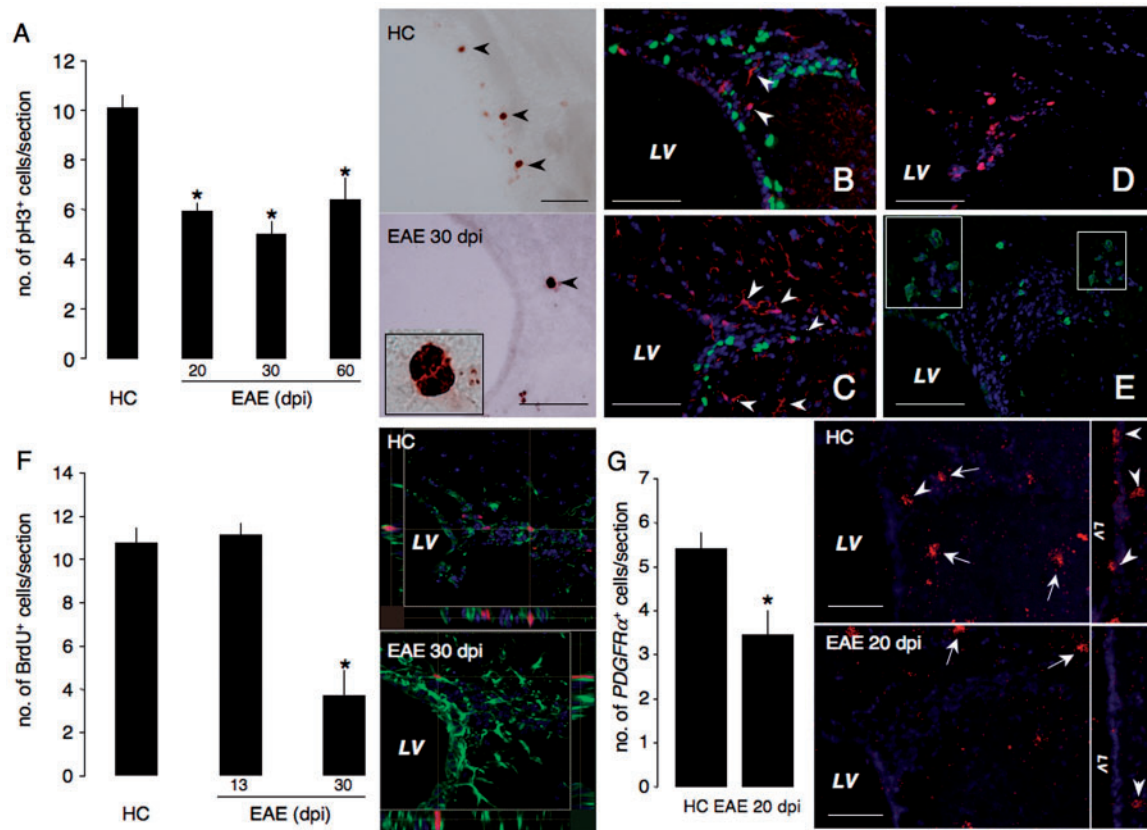


Fig. 1 Chronic autoimmune CNS inflammation impairs proliferation of SVZ-resident NPCs *in vivo*. **(A)** Decrease of M-phase confined phosphorylated histone H3 (pH3)⁺ cells is observed in the SVZ of EAE mice at both 20, 30 and 60 dpi. Data in the graph are represented as mean numbers of pH3-immunoreactive cells/section ± SEM and have been obtained from a total of $n \geq 5$ mice per group. * $P \leq 0.05$, when compared with HC. Two representative images of pH3⁺ cells in the SVZ of HC and EAE 30 dpi are shown. Scale bars 50 μ m. **(B–E)** Coronal sections of the dorsolateral SVZ from HC mice **(B and D)** and mice with EAE at 30 dpi **(C and E)** showing fast-proliferating IddU⁺ cells (green in **B and C**), IddU⁺/Ibal⁺ (green and red in **B and C**, respectively) and CD45⁺/Ki67⁺ (green and red in **D and E**, respectively) cells in EAE vs. HC. Arrowheads indicate IddU⁺/Ibal⁺ cells in both panels. Scale bars: 50 μ m. **(F)** Decrease of long-term BrdU-retaining cells is observed in the SVZ of EAE mice at 30 dpi. Mice received BrdU for 6 days starting from either 13 or 30 dpi and were sacrificed 40 days after the last BrdU injection. Data are represented as mean numbers of BrdU⁺ cells/section ± SEM and have been obtained from a total of $n \geq 3$ mice per group from $n \geq 2$ independent experiments. * $P \leq 0.001$, when compared with HC. Two representative confocal microscopy pictures showing long term-retaining BrdU⁺ (red) GFAP⁺ (green) cells from the SVZ of HC and EAE 30 dpi are shown. **(G)** Decrease of SVZ cells expressing the mRNA for *PDGFR α* is observed in the SVZ of EAE mice at 20 dpi. *PDGFR α* mRNA is expressed by putative type slow-dividing cells located within the SVZ, as well as by OPCs that are widely distributed within the adult brain parenchyma (arrowheads in the upper panel). Data are represented as mean numbers of *PDGFR α* ⁺ cells/section ± SEM and have been obtained from a total of $n \geq 3$ mice per group. Scale bars: 50 μ m. Nuclei in **(B–G)** have been counterstained with DAPI. LV, lateral ventricle.

In HC, type A cells were usually elongated (migratory morphology), while they showed a more spherical shape in EAE mice at 30 dpi. Also the characteristic dense contacts between type A cells (Doetsch *et al.*, 1997) were less evident in the SVZ of EAE mice (Supplementary Fig. 2).

Occasionally, this caused the non-migratory type A cells to protrude into the ventricular cavity that appeared bordered by two layers of type E cells (Fig. 2B), while some clusters of type A cells appeared to divert their migration out of the SVZ through the striatum, following blood vessels (data not shown).

Despite the lack of altered morphology in the different SVZ cell types in EAE mice, the multifocal derangement of the SVZ cytoarchitecture was substantial. Some regions of

the SVZ of EAE mice at 30 dpi showed focal accumulation of up to six to seven layers of type A cells at the ventricular lumen interface, while HC usually display only two layers of type A cells (Fig. 2C and D).

To quantify these changes (see also Supplementary Fig. 2 and Supplementary data), we calculated the percentage of distinct SVZ cell types from EAE and HC mice by EM. There was a 39–46% decrease of type C cells at 10 dpi ($6.8 \pm 1.5\%$) and 20 dpi ($6.1 \pm 0.7\%$), compared with HC ($11.2 \pm 0.7\%$, $P \leq 0.001$). A 2- to 8-fold decrease in the number of mitoses was also found in EAE both at 10 dpi ($0.1 \pm 0.07\%$) and 30 dpi ($0.43 \pm 0.1\%$) compared with HC ($0.81 \pm 0.1\%$, $P \leq 0.05$). The percentage of type C cells ($9.5 \pm 0.9\%$) and the mitoses ($0.95 \pm 0.2\%$) returned toward baseline values in

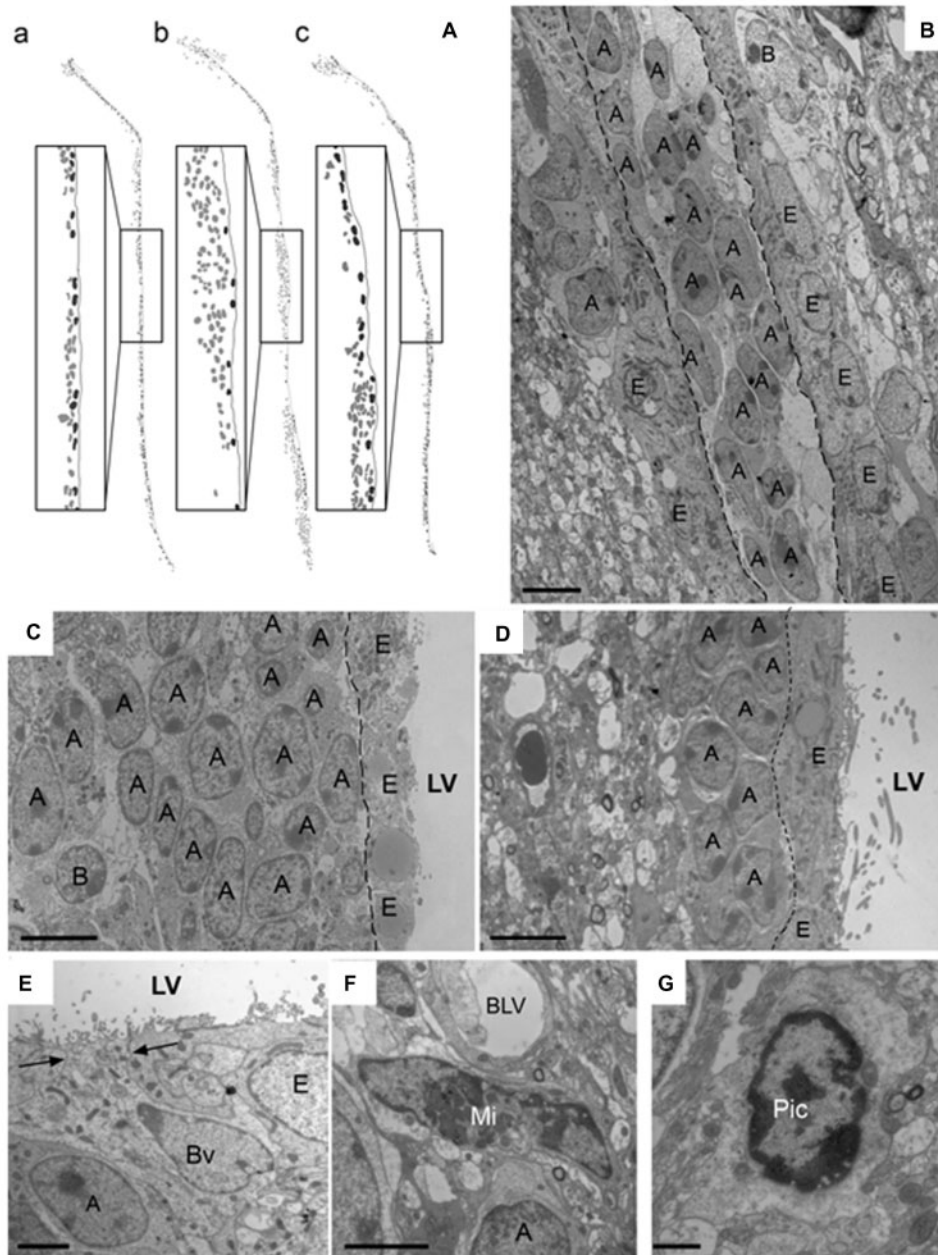


Fig. 2 Chronic autoimmune CNS inflammation impairs cell organization in the SVZ germinal niche. **(A)** Diagrams of cell organization along the SVZ of HC (a) and EAE mice at 30 (b) and 60 dpi (c). Representative areas are shown at higher magnification. Note the homogeneous organization in HC, while in EAE mice at 30 dpi, cells accumulate and form large cell clusters. These clusters tend to recover at 60 dpi. Ependymal cells are depicted in black, while SVZ cells in grey; **(B)** Transmission EM of the EAE SVZ region at 30 dpi. A chain of migrating neuroblasts (**A**) appears in the lateral ventricle (LV), delimited with a discontinuous line. Ventricle walls are covered by ependymal cells (**E**); **(C)** EAE mice at 30 dpi show large cell clusters, composed of several layers of accumulated migrating cells (**A**); **(D)** The HC SVZ shows a homogeneous group of migrating neuroblasts (**A**). Arrows indicate the typical free spaces between type A cells, which become less noticeable in EAE mice; **(E)** Representative images of a single type B cell or astrocyte (**B**) touching the ventricular cavity (LV) through an expansion (arrows). These astrocytes might be activated in response to proliferation signals and tend to disappear within the SVZ of EAE mice; **(F)** Representative image of a single microglial cell (Mi). Some of these cells are filled with dense bodies, are frequently located in close proximity to blood vessels (BLV) and tend to increase in the SVZ of EAE mice at 10–30 dpi; **(G)** Picnotic cells (Pic) are transiently increased in the SVZ of EAE mice. Scale bars in **B**, **C** and **D**: 5 μ m, while in **E** and **F**: 2 μ m.

EAE mice at 60 dpi. Furthermore, we found almost a 2-fold increase in perivascular (activated) microglial cells in EAE mice at 20 dpi ($0.56 \pm 0.3\%$) compared with HC ($0.35 \pm 0.1\%$) (Fig. 2F). Finally, picnotic cells in EAE mice

were significantly increased only at 20 dpi ($1.12 \pm 0.5\%$), compared with HC ($0.3 \pm 0.06\%$, $P \leq 0.05$) (Fig. 2G). The relative percentages of ependymal cells, astrocytes and neurons did not vary among groups.

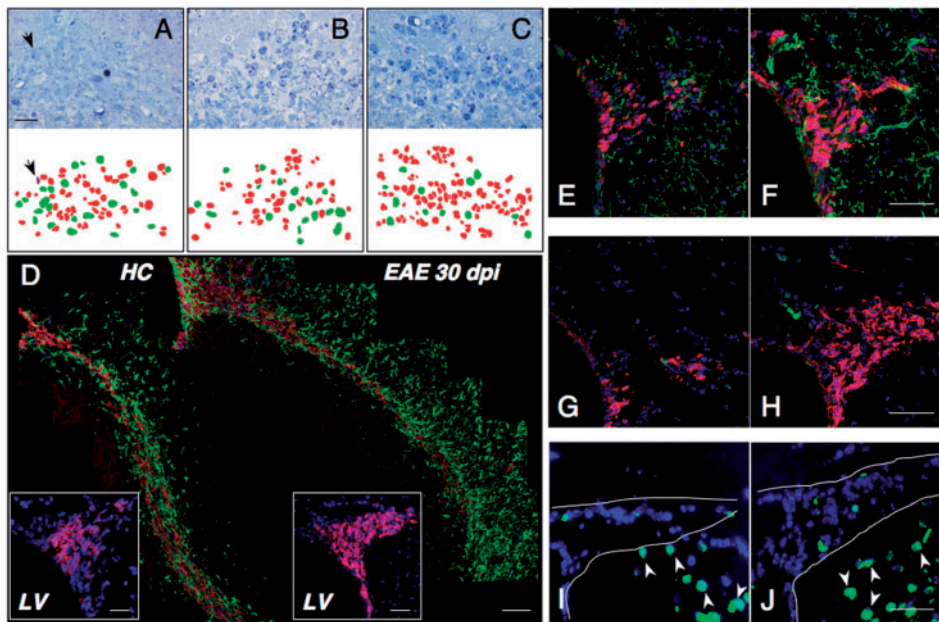


Fig. 3 Chronic autoimmune CNS inflammation impairs migration of SVZ neuroblasts. (A–C) Representative toluidine blue-stained semi-thin sections of the RMS of EAE mice at 30 (A) and 60 dpi (B) and HC (C). The same sections were taken-off, and ultrathin sections were re-cut. Cells were studied at the EM and identified as neuroblasts or astrocytes (red and green in lower panels). Note the disorganization of the RMS of EAE mice at 30 dpi (A), with significantly low numbers of migrating neuroblasts and numerous astrocytes. The RMS of EAE mice at 60 dpi showed a trend to recovery normal morphology (B), as compared with HC (C). The arrow at 30 dpi shows a microglial cell (purple). Scale bar: 20 μm. (D) Sagittal reconstructions of the whole RMS from a representative HC (left panel) and a mouse with EAE at 30 dpi (right panel). Migratory neuroblasts are detected by PSA-NCAM (red), while astrocytes are detected by GFAP (green). Note normal PSA-NCAM⁺ chains of migratory cells in the HC mouse (left panel). In contrast, the PSA-NCAM⁺ cells in the RMS of EAE mice at 30 dpi appear deranged in their migratory path toward olfactory bulbs (right panel). EAE mice also display increased numbers of GFAP⁺ astrocytes within the parenchyma surrounding the RMS. Coronal sections show clear disorganization of migratory chains with less PSA-NCAM⁺ neuroblasts (purple cells in the magnified inset) at the dorsal SVZ level in EAE mice. Nuclei in magnified insets have been counterstained with DAPI. Scale bars: 50 μm. LV = lateral ventricle. (E–J) Coronal brain sections showing double immunofluorescence for PSA-NCAM (red) and NG2 (green in E and F) or Olig2 (green in G and H). Note the absence of co-staining for both NG2 and Olig2 in EAE mice at 30 dpi (F and H) and HC (E and G). In I and J, NeuN staining (green) is shown in a HC mouse (I) and in a EAE mouse (J) at 30 dpi, respectively. Note that very few cells are stained in the SVZ (surrounded by a continuous line) of both mice while the majority of striatal neurons are stained (arrowheads). In all panels, nuclei have been counterstained with DAPI and the scale bar is 100 μm.

Migratory defect of neuroblasts in the rostral migratory stream of EAE mice

We then hypothesized that an alteration of the migratory capacity of type A cells—with non-migratory neuroblasts accumulating in the SVZ—was occurring in EAE mice as a consequence of persistent CNS inflammation. To address this issue we performed semithin section analysis of the rostral migratory stream (RMS) in EAE versus HC mice.

We found that the RMS of EAE mice at 30 dpi was profoundly disorganized (Fig. 3A), with significantly less migrating neuroblasts (Fig. 3A, red cells in lower panel) and more numerous astrocytes (Fig. 3A, green cells in lower panel). The RMS of EAE mice at 60 dpi (Fig. 3B) showed a trend to recovery to normal morphology (Fig. 3C). EM confirmed cell identities in the RMS of both groups of mice (data not shown). Accordingly, in EAE mice at 20 and 30 dpi, immunofluorescence analysis of sagittal brain sections revealed increased accumulation of PSA-NCAM⁺ neuroblasts within the more rostral SVZ, which were not

clustered in tight rows as detected in HC but appeared scattered within the RMS, possibly indicating migratory defects (Fig. 3D, magnified insets). Indeed, the astrocytic glial tubes surrounding the RMS in EAE mice appeared disrupted with accumulation of GFAP⁺ cells either inside the RMS or in the lateral parenchyma.

We also investigated whether the observed accumulation of non-migratory neural progenitors might mask a switch towards oligodendro- versus neuro-genesis. We did not find evidence of PSA-NCAM⁺ cells co-expressing any of the two putative markers of OPCs, NG2 (Fig. 3E and F) and Olig2 (Fig. 3G and H). Furthermore, laser-capture microdissection (LCM)-based gene expression analysis of major (oligodendro)glial cell fate determinants (e.g. *Olig1*, *Olig2*, *Nkx2.1*, *Nkx2.2*) in the SVZ, showed no differences between EAE 20 dpi and HC (Supplementary Fig. 3). Similarly, we did not find at 30 dpi any increase of mature NeuN⁺ neurons within the SVZ (Fig. 3I and J). This latter finding was also confirmed by EM analysis showing a non-significant difference between the number of SVZ

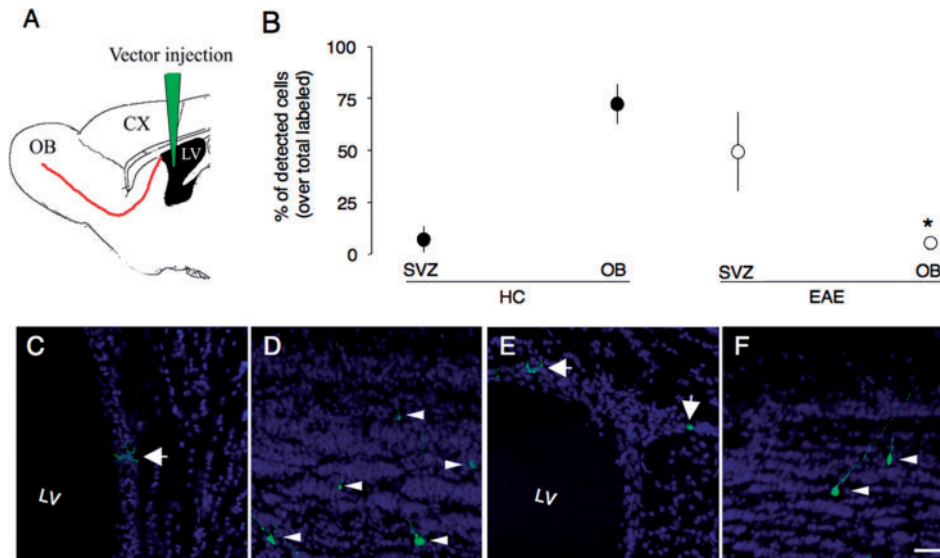


Fig. 4 Retroviral cell tracing shows impaired migratory behaviour of SVZ progeny. **(A)** A replication-defective retrovirus expressing the green fluorescent protein (GFP) was injected stereotactically in the lateral ventricle so to infect S-phase confined cells. The green line shows the needle track, while the red line indicates the RMS. Nineteen days after the injection, GFP⁺ cells migrating along the RMS were numbered in a region spanning from the anterior SVZ to the OB. OB, CTX = cortex; LV = lateral ventricle. **(B)** EAE mice display a significant reduction of the subset of GFP⁺ cells migrating to the OB and an increase in non-migrating GFP⁺ cells detected very close to the SVZ, when compared with HC. Data are expressed as mean percentage of detected cells (over total labelled) \pm SEM from $n = 3$ mice per group. * $P \leq 0.05$. **(C–F)** GFP⁺ cells (green) are detected both in the SVZ lining and in the OB from HC **(C and D)** and EAE at 20 dpi **(E and F)**. The arrows in **C** and **E** indicate SVZ GFP⁺ cells. The arrowheads in **D** and **F** show OB GFP⁺ cells. Nuclei are counterstained with DAPI. Scale bar: 150 μ m. LV, lateral ventricle.

neurons in HC (0.34 ± 0.1) versus EAE at 30 dpi (0.57 ± 0.2 ; $P = \text{NS}$).

Finally, we directly analysed how the newly generated SVZ cells migrate towards physiological (e.g. the OB) routes of migration. To do this we used a replication-defective retrovirus expressing the green fluorescent protein (GFP). The vector was injected into the right ventricle of both HC and EAE mice at 20 dpi and the number of GFP⁺ cells was quantified 19 days after the injection in a region spanning from the anterior SVZ to the OB (Fig. 4A). When compared with HC, EAE mice showed a significant ($P \leq 0.05$) reduction of GFP⁺ cells migrating tangentially along the RMS up to the OB and differentiating into granule and periglomerular neurons (Fig. 4B). In contrast, we did not observe any quantitative difference—between EAE 20 dpi and HC—in the subset of non-migrating GFP⁺ cells being detected at the level of the SVZ (Fig. 4B–F).

These results provide evidence of a prominent migratory impairment and exclude the occurrence of a switch towards (oligodendro)gliogenesis of the newly generated SVZ progeny in EAE mice.

Impaired clonal efficiency of NPCs from EAE mice *in vitro*

We next studied the self-renewal of CNS stem/progenitor cells by using an *ex vivo* assay. It has been shown that neurosphere-forming cells consist mostly of type C (and type B) cells *in vitro* (Morshead *et al.*, 1994). Therefore,

we used the classical *in vitro* NS-A to further characterize the SVZ stem cell population of EAE mice, with the numbers of clonal neurospheres *in vitro* as a measure of the absolute number(s) of putative stem cells *in vivo* (Reynolds and Weiss, 1992; Morshead *et al.*, 1994).

Neurospheres (both primary and secondary) from EAE mice did not show differences in size at any time point, compared with neurospheres from both HC and CFA-immunized mice (Supplementary Fig. 4), thus suggesting that SVZ stem cells from symptomatic EAE mice do not differ in their mitogenic capacity from cells derived from controls. However, the clonal efficiency of SVZ primary neurospheres—while comparable between asymptomatic (e.g. 10 dpi) EAE mice and HC—became different once clinical EAE started. In fact, significantly less primary neurospheres were derived from EAE mice at 20, 30, 60, 120 and 240 dpi (all $P \leq 0.0001$), when compared with controls (Fig. 5A).

This decline in clonal efficiency was confirmed in secondary neurospheres at the same time points (Supplementary Fig. 4), further corroborating the previous *in vivo* observation that significant impairment of the SVZ stem/precursor cell compartment occurs at certain time points of chronic EAE in mice. Interestingly, *in vitro* extended culturing of neurospheres from EAE mice with FGF-II and EGF for a total of 10 passages of amplification completely reversed the impairment of clonal efficiency observed in primary and secondary neurospheres (Fig. 5B). In order to solve some of the limitations of the classical NS-A (Bull and Bartlett, 2005;

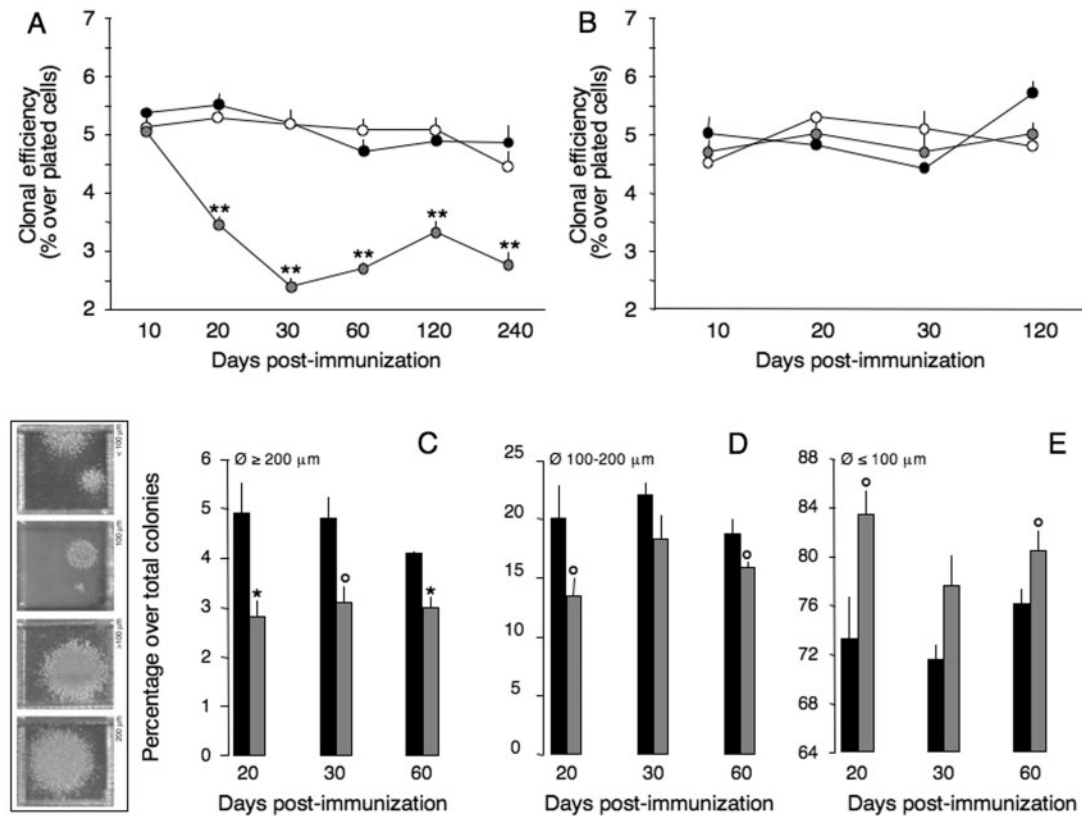


Fig. 5 Neurospheres from mice with chronic autoimmune CNS inflammation display reduced self-renewal. **(A)** Quantitative analysis of clonal efficiency of HC (black circles) and CFA-immunized controls (white circles) as well as EAE mice (grey circles). Note the significant and persistent impairment of clonal efficiency of primary neurospheres from EAE mice at 20, 30, 60, 120 and 240 dpi, when compared with controls. **(B)** The clonal efficiency of primary neurospheres from EAE mice is completely reverted after $n = 10$ passages of amplification *in vitro* and it is comparable HC and CFA-immunized controls. A total of three to six mice per group per experiments were analysed per time point. Data are represented as mean clonal efficiency \pm SEM from a total of $n \leq 3$ independent experiments. $**P \leq 0.0001$. **(C–E)** Neural Colony Forming Cell (NCFCA) assay-based quantification of large- **(C)**, medium- **(D)** and small-sized **(E)** colonies. Note the significant and persistent reduction of large- and medium-sized colonies, while increase in small-sized colonies in EAE mice (grey bars), when compared with HC (black bars). Data are represented as mean percentage of colonies \pm SEM over the total number of plated cells from a total of $n \geq 3$ independent experiments. A total of six mice per group per experiments were analysed per time point. $*P \leq 0.05$; $^{\circ}P \leq 0.005$. \emptyset , colony diameter.

Singec *et al.*, 2006), we repeated the *in vitro* quantification of stem-like cells by using a size-based NCFCA, which has been recently developed to differentiate between colonies formed by *bona fide* neural stem cells from those formed by progenitor cells, based on their different proliferative potential *in vitro* (Louis *et al.*, 2008). A significant decrease in large-size neural colony-forming cells (with putative large self-renewal capacity) (Fig. 5C, $P \leq 0.05$ at both 20, 30 and 60 dpi) as well as medium-sized colonies (with putative limited self-renewal capacity) (Fig. 5D, $P \leq 0.05$ at both 20 and 60 dpi) was observed in cells from the SVZ of EAE mice, when compared with HC. In parallel, a significant increase of small-size colonies (with low, if any, self-renewal capacity) (Fig. 5E, $P \leq 0.05$ at both 20 and 60 dpi) was also found in the cells from the SVZ of EAE mice, when compared with HC. Interestingly, the major *in vitro* biological properties of SVZ stem cells from the SVZ of EAE mice—namely proliferation with mitogens, self-renewal and multipotency upon mitogen removal—were not significantly altered,

when compared with both HC and CFA-immunized controls (Supplementary Fig. 5).

While further confirming that inflammation occurring during EAE significantly impairs the kinetics of both slow and fast proliferating SVZ cells, the *in vitro* data also suggested that the chemically defined growth factor-enriched (FGF-II plus EGF) microenvironment into which neurospheres are grown might be *per se* sufficient to re-establish the observed cell non-autonomous dysfunction.

Inflammation-dependent deregulation of cell cycle progression

In order to elucidate some of the molecular mechanism(s) underlying the inflammation-induced failure of SVZ cells, we performed a wide TaqMan[®] Low-Density Array (TLDA)-based gene expression profiling in the acutely dissociated SVZ of EAE mice at different time points (e.g. 10, 20, 30 and 120 dpi). One hundred and sixty-seven different mRNA

species involved in stemness, inflammation, immunity, self-renewal, differentiation and migration were measured (see Supplementary information). Differences in gene expression were mostly seen in EAE at 20 and 30 dpi ($r^2 = 0.60$ and $r^2 = 0.59$, respectively), when compared with 10 and 120 dpi (both $r^2 = 0.92$) (Supplementary Fig. 6).

Interestingly, 60.5% (101/167) and 27.5% (46/167) of screened genes either did not change at any time point or were not expressed at more than one time point, respectively. Only 9% (15/167) of screened genes were up regulated in the SVZ of EAE mice at 20 and/or 30 dpi, when compared with HC. On the other hand, 3% (5/167) of the genes were down-regulated in the EAE mice among which we identified at least two major markers for stem/precursor cells of the SVZ germinal niche, such as *Prominin-1* and *Tenascin-C* (Martino and Pluchino, 2006) (Fig. 6A). According to LCM analysis of the SVZ (Supplementary Fig. 3), we did not find any up regulation of (oligodendro)glial cell fate gene determinants, such as *Nkx2.2* (Fig. 6A and B).

Among up-regulated genes, the most prominent were inflammatory regulators (e.g. *CCL5/Rantes*, *CXCL10/IP-10* and *Heme-oxygenase1*), a transcription factor downstream the IFN- γ signalling (e.g. *STAT-1*), a number of cell cycle regulators (e.g. *Cdc2a/p34*, *Cdkn1a/p21* and *Cdkn1c/p57*), and two neuronal-lineage specific transcription factors (e.g. *Dlx1* and *Dlx2*) (Fig. 6B). As an *in vivo* confirmation of these latter data, an increased number of cells expressing *Cdkn1a/p21*⁺ and *Dlx2*⁺ mRNA cells was observed in the SVZ of EAE mice at 30 dpi, compared with HC (Fig. 6C–F).

Induction of quiescence of SVZ NPCs *in vitro* by inflammatory cytokines

The gene expression pattern in the SVZ of EAE mice supports the idea that the impairment of proliferation and migration, we observed *in vivo*, might have occurred as a consequence of a CNS-confined inflammatory process leading to cell cycle deregulation. We found a significant up-regulation of mRNA levels for pro-inflammatory (Th1) cytokines, such as interferon (IFN)- γ and tumour necrosis factor (TNF)- α (Fig. 6G and H, respectively), but not of interleukin (IL)-1 β (Fig. 6I), at 20 and 30 dpi in the SVZ from EAE mice ($P \leq 0.005$, when compared with CFA-immunized mice). Given the central role played by Th1 cytokines in triggering and perpetuating chronic inflammation in EAE, we thus hypothesized that Th1 cytokines might have contributed to the impaired proliferation of stem/precursor cells observed in the SVZ of EAE mice. Primary SVZ cells from HC were grown in the continuous presence of Th1 (e.g. IFN- γ , TNF- α and IL-1 β) or Th2 (e.g. IL-4, IL-5 and IL-13) cytokine mixes. When plated in presence of Th1, but not Th2, cytokines SVZ cells showed dramatic impairment in the formation of large-size neural colony-forming cells ($P \leq 0.0001$, when compared with control SVZ cells). This was paralleled by a significant increase of small-sized colonies with low self-renewal capacity

($P \leq 0.05$, when compared with control SVZ cells). The observed results were not obtained when cytokines of either type were added to the SVZ cell assay only for 48 h (Fig. 7A). To confirm whether NPC self-renewal could be affected by inflammatory Th1 cytokines, we generated continuous growth curves of neurospheres cultured in complete growth medium (CGM), or in CGM enriched with either Th1 or Th2 cytokines. Only neurospheres cultured in Th1-enriched CGM showed progressive and significant (from two to six passages of amplification) decrease of growth efficiency (Fig. 7B, all $P \leq 0.05$, when compared with control neurospheres), while no difference was observed in neurospheres cultured in Th2-enriched CGM. Interestingly, as early Th1 cytokines were removed from the CGM and cell amplification was carried on for $n = 6$ further passages of amplification, the growth efficiency of neurospheres previously exposed to cytokines returned to control values (Fig. 7C). Among Th1 cytokines, IFN- γ —but not TNF- α and IL-1 β —seemed to play a crucial role in the impairment of long-term proliferating capacity of neurospheres ($P \leq 0.05$, when compared with control neurospheres) (Fig. 7D). As a further confirmation, we found that exposure of SVZ NPCs to Th1 but not Th2 cytokines lead to significant increase (33–46%) of cells in the G₀/G₁ phase ($P \leq 0.005$) and to a parallel decrease of cells in the S phase ($P \leq 0.005$), when compared with controls. No difference was observed in G₂/M phase-restricted cells between groups (Fig. 7E).

We then sought to analyse in more details the growing fractions of cytokine-conditioned NPCs as determined by the expression of the Ki67 antigen, a molecular marker that is expressed exclusively in proliferating cells during the late G₁, S, G₂ or M phase of the cell cycle. Accordingly, a significant increase in the percentage of Ki67⁺ G₀-phase confined quiescent NPCs—representing the $70.6 \pm 1.9\%$ of the cultured cell population—was observed upon exposure of NPCs to Th1 but not Th2 cytokines (Figure 7F, $P \leq 0.0001$, when compared with both control and Th2-conditioned neurospheres). Cell apoptosis assessed by Annexin/PI staining did not account for any of the observed phenomena (data not shown).

Alteration of SVZ cell cycle by inflammatory cytokines *in vivo*

To further investigate the role played by pro-inflammatory cytokines in deregulating the cell cycle of NPCs *in vivo*, we analysed the SVZ of HC and EAE mice upon stereotactical injection of a Th1 cytokine mix (e.g. TNF- α and IFN- γ) in a brain area close to the SVZ, as previously described (Merkler *et al.*, 2006). Mice were sacrificed 3 and 10 days after cytokine injection and *in vivo* cell cycle analysis was performed using systemic IddU to label proliferating cells. Severe impairment of SVZ fast-proliferating transit amplifying precursors (type C cells) was found in TNF- α /IFN- γ -injected HC ($P \leq 0.005$, when compared with untreated HC mice) (Fig. 7G). Similarly, IddU⁺ precursors

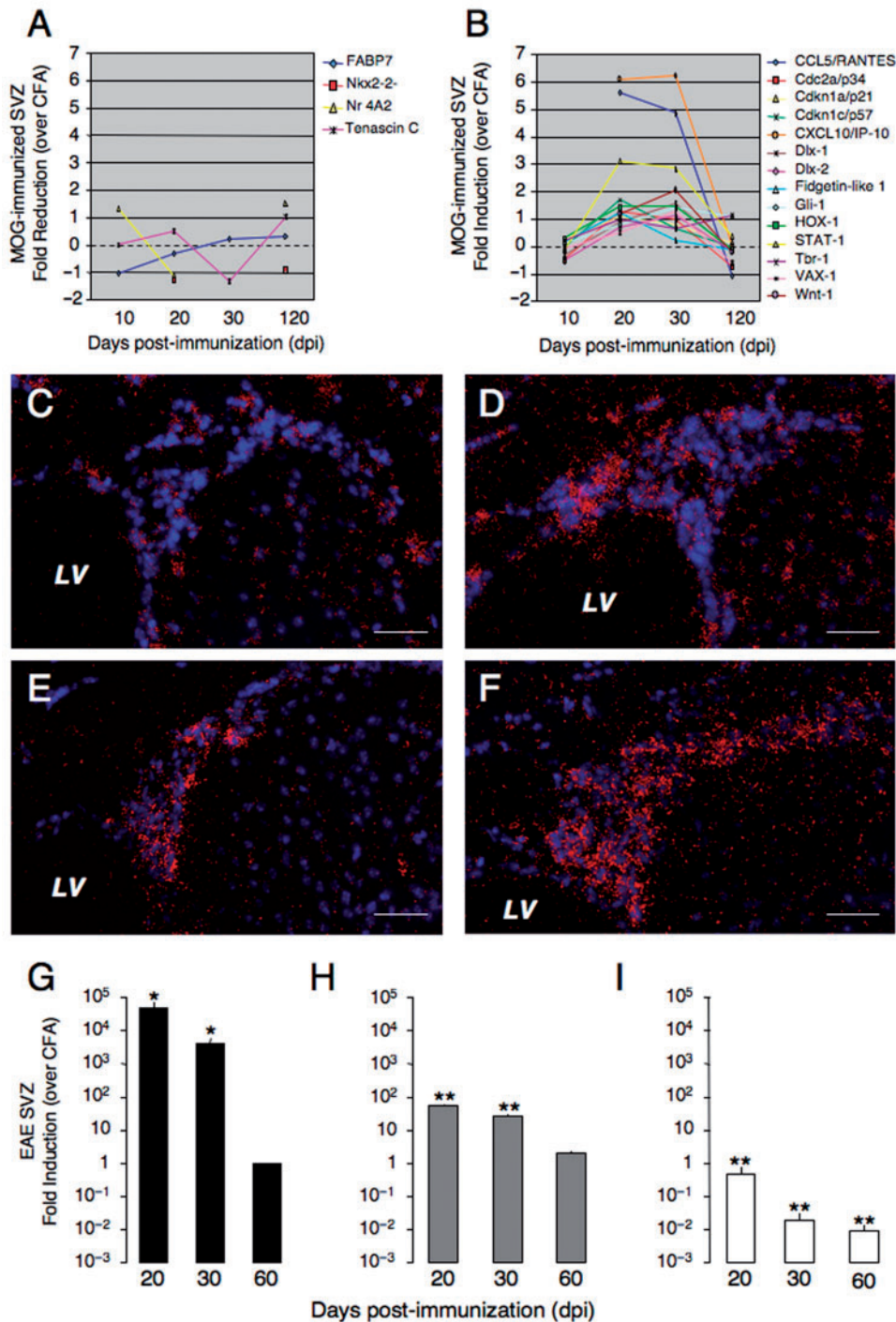


Fig. 6 CNS inflammation induces expression of cell cycle regulators and neurogenic transcription factors at mRNA level. **(A, B)** Semi-quantitative analysis of selected mRNAs. The graph in **A** includes a list of $n = 5$ selected genes showing significant down-regulation (fold reduction ≥ 1) at any time point in the SVZ of EAE mice, when compared with CFA-immunized controls. The graph in **B** includes a list of $n = 15$ selected genes showing significant up-regulation (fold induction ≥ 1) at any time point in the SVZ of EAE mice, when compared with CFA-immunized controls. **(C–F)** *In situ* hybridization for *Dlx2* (**C** and **D**) and *Cdkn1a/p21* (**E** and **F**) on coronal brain sections from both HC (**C** and **E**) and EAE 30 dpi (**D** and **F**). EAE mice show increased numbers of *Dlx2*⁺ and *Cdkn1a/p21*⁺ cells within the SVZ, when compared with HC. Autoradiographic grains (red) were captured with 20 \times objective in a dark field light microscopy and tissue was visualized by DNA staining (DAPI, blue). LV = lateral ventricle. Scale bars: 50 μ m. **(G–I)** Significant increase of IFN- γ and TNF- α mRNA levels (**G** and **H**, respectively) in the SVZ of EAE mice at 20 and 30 dpi compared with CFA-immunized controls. The graph in **F** shows the significant decrease of *IL-1 β* mRNA levels in the SVZ of EAE mice at 20 and 30 dpi. Data are represented as mean arbitrary units \pm SEM and have been obtained in single from the SVZs of $n \geq 6$ per mice per group per time point. * $P \leq 0.05$; ** $P \leq 0.0001$.

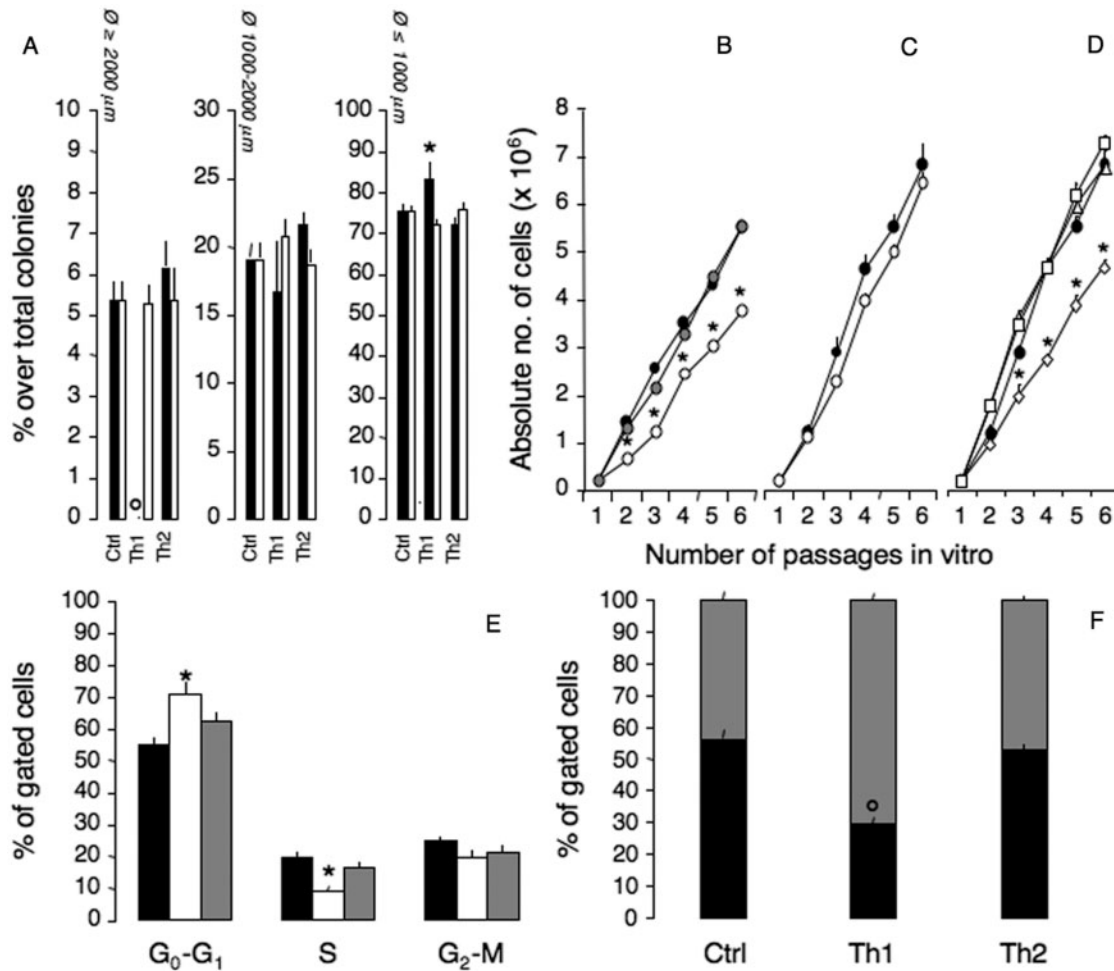


Fig. 7 Chronic CNS inflammation induces quiescence of neural stem cells *in vitro* and *in vivo*. **(A)** NCFC assay performed on primary SVZ NPCs in the presence of either Th1 cytokines (IFN- γ , 500 U/ml; TNF- α , 200 U/ml; IL-1 β 100 U/ml) or Th2 cytokines (IL-4, IL-5 and IL-13, all 10 ng/ml). SVZ cells were plated at clonal density in cytokine-enriched NeuroCult for either the last 48 h (white bars) or for the whole length of the assay (black bars). No difference in the percentage(s) of generated colonies were found upon 48 h of conditioning either with Th1 or Th2 cytokines, while longer (3 weeks) Th1 cytokine conditioning induced a complete failure of the generation of large-size colonies. Data are represented as mean percentage of colonies/size over total plated cells \pm SEM and have been obtained from a total of $n \geq 3$ independent experiments. $*P \leq 0.0001$; $*P \leq 0.05$. **(B–D)** Proliferation analysis of NPCs grown *in vitro* with CGM enriched with cytokines. **(B)** Th1 (white circles) or Th2 cytokines (grey circles) are compared with CGM alone (black circles). Note the significant decrease of proliferation rate of Th1 conditioned cells appearing as early as after $n=2$ passages of amplification, while no difference was observed in neurospheres cultured in Th2-enriched CGM. **(C)** After Th1 cytokines withdrawal, NPCs are kept growing in CGM alone for further $n=6$ passage of amplification and no differences in growth efficiency are observed when previously exposed NPCs to Th1 cytokines (white circles) are compared with control NPCs (black circles). **(D)** Proliferation analysis of NPCs grown *in vitro* in CGM enriched with single Th1 cytokines. IFN- γ alone (white diamonds) induces a significant reduction of growth rate (from four to six passages of amplification), while cells conditioned with either TNF- α or IL1- β do not show difference in growing efficiency at any time point. Data are represented as absolute numbers of cells \pm SEM from a total of $n \geq 3$ independent experiments. $*P \leq 0.05$, when compared with controls. **(E)** NPCs were cultured for 48 h in CGM enriched with either Th1 (white bars) or Th2 cytokines (grey bars). NPCs cultured in CGM alone were used as controls (black bars). Note the significant shift (33–46% of cells) in the cells toward G_0/G_1 , and a decline in cells in S phase upon exposure to Th1 but not Th2 cytokines. Data are represented as mean percentage of gated cells \pm SEM for a total of $n \geq 5$ independent experiments. $**P \leq 0.05$, when compared with controls. **(F)** FACS analysis for Ki67. Note the significant increase of G_0 -confined Ki67 $^+$ cells (grey bars) in Th1 cytokine-conditioned but not in unconditioned (Ctrl), or Th2-cytokine conditioned NPCs. Black bars indicate Ki67 $^+$ cell. Data are represented as mean percentage of gated cells \pm SEM for a total of $n \geq 10$ independent experiments. $P \leq 0.0001$, when compared with controls. **(G)** Significant reduction of the GF upon focal injection of IFN- γ /TNF- α into the dorsolateral SVZ was observed in both HC or EAE 20 dpi mice 3 days (grey bars) after cytokine injection, compared with baseline values. Ten days after cytokine injection (white bars), the GF still remained significantly lower than normal values in HC only. NPCs proliferation was assayed by continuous exposure to systemic IddU for a total of 10 h before the sacrifice and evaluated by counting only IddU $^+$ /Iba1 $^-$ (green and red cells in the panels, respectively) cells in the SVZ. Black bars represent baseline time points. Data are represented as mean labelling index (L.I.) \pm SEM from a total of $n \geq 3$ mice. In the panels, images of the SVZs of two representative HC and EAE mice injected with IFN- γ /TNF- α are shown. Nuclei are counter-stained with DAPI. Scale bars: 50 μ m. $*P \leq 0.05$; $**P \leq 0.005$. LV = lateral ventricle.

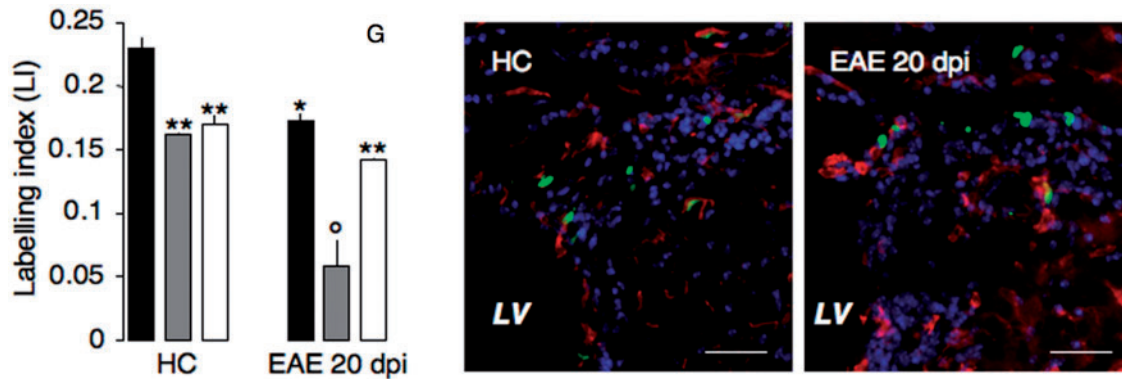


Fig. 7 Continued.

were further reduced in TNF- α /IFN- γ -injected EAE mice as compared with untreated EAE mice ($P \leq 0.05$). This phenotype was partially reversed as early as 10 days after the initial cytokine injection (Fig. 7G), the expected half-life of molecules such as cytokines *in vivo*.

Discussion

Here we show a significant decrease of proliferation of both fast cycling (type C cells) and slowly dividing (type B cells) cells accompanied by an increase of newly generated non-migratory neuroblasts (type A cells) in the SVZ of EAE mice during the peak of CNS-confined chronic inflammation. This alteration is associated with *in vitro* and *in vivo* changes: the expression of the cyclin-dependent kinase inhibitor Cdkn1a/p21 (Gartel *et al.*, 1996) is increased in the SVZ from EAE mice; SVZ-derived neurospheres from EAE mice display low clonal efficiency; and the percentage of Ki67⁻ G₀ phase-confined quiescent NPCs increases up to 70% upon exposure to pro- (Th1) but not anti- (Th2) inflammatory cytokines. These results suggest that persistent CNS inflammation significantly alters the cell kinetics of precursors and stem cells residing within the SVZ germinal niche by inhibiting their entry into the cell cycle by up-regulation of cell cycle inhibitors.

While the central role played by chronic inflammation in decreasing the GF of SVZ cells is confirmed by the fact that the proliferation capacity of fast cycling cells tends to return to normal values in EAE mice as early as inflammation fades out (from 60 dpi on), it is less clear why there is a parallel accumulation of neuroblasts within the SVZ. Here we provide direct evidence for the inability of SVZ cells to migrate tangentially along the RMS up to the OB within a chronically inflamed microenvironment. This latter finding, along with the EM evidence of a preserved morphology but altered location of SVZ cells in EAE, prompts us to hypothesize that persistent CNS-confined inflammation might also affect the parenchymal astrocytes forming the glial tubes within the RMS and, as a consequence, alter the migratory capacity of the SVZ progeny (the newly generated PSA-NCAM⁺ cells). Likewise, it would be also very likely that

some neuroblasts divert their physiological rostral migration towards more caudal inflammatory lesions in the corpus callosum, as previously suggested (Picard-Riera *et al.*, 2002).

Interestingly, clonal efficiency of SVZ-derived neurospheres is significantly lower at the peak of inflammation in EAE mice but returns to normal values upon extensive *in vitro* culturing with growth factors. This result—which agrees with the *in vivo* evidence showing that SVZ resident cells tend to behave normally as soon as CNS inflammation abates—suggests that certain cell non-autonomous factors may transiently alter NPC self-renewal both *in vivo* and *in vitro*. Among such factors, pro-inflammatory cytokines seem to play a major role. We found that IFN- γ induces alteration of NPC kinetics *in vitro* and Stat-1—which belongs to IFN- γ intracellular signalling pathway (Robinson and O'Garra, 2002)—is up-regulated in SVZ from EAE mice during the peak of inflammation. Furthermore, IFN- γ is also able to restrict NPC cell cycle progression to the G₀ phase *in vitro* and to impair proliferation of SVZ cells *in vivo*. These IFN- γ -mediated effects are transient, reversible, not associated with induction of apoptosis, and supported by previous evidence. It has been previously shown that types I and II IFNs can affect the growth of different cell types through the Janus kinase-signal transducers and activators of transcription pathway and in particular through the activation of the transcription factor Stat-1 (Bromberg *et al.*, 1996). The central role played by inflammatory molecules in altering NPC self-renewal is also supported by the impairment of hippocampal neurogenesis induced by the pro-inflammatory cytokine IL-6 (Monje *et al.*, 2003).

The effects described here are relevant to the specific brain disease model we have examined, and it is likely that different types of brain damage (e.g. ischaemic stroke, neurodegenerative diseases, etc.) may induce opposite findings (Calza *et al.*, 1998; Picard-Riera *et al.*, 2002; Zhang *et al.*, 2004; Jin *et al.*, 2006; Nait-Oumesmar *et al.*, 2007), such as the recent demonstration that different inflammatory players (e.g. IL-4 and IFN- γ) or immune cells themselves may variably support either glio- or neuro-genesis (Butovsky *et al.*, 2006; Ziv *et al.*, 2006).

Thus, in this model, persistent CNS-compartmentalized inflammation mediates changes in the SVZ cells that recover when inflammation abates. What would be the outcome of recurrent bouts of inflammation as might be seen in relapsing-remitting multiple sclerosis? Other models of EAE (such as the SJL/J model) will need to be evaluated to answer this question. It would also be interesting to determine whether the defect in the SVZ cell proliferation will continue to be reversible after multiple inflammatory attacks. Further studies will be needed in order to clarify whether recurrent hits of inflammation induce permanent changes in the SVZ that would then lead to irreversible failure of the homeostatic and repair capabilities of the endogenous neural stem/precursor cell compartment. Our findings have implications for therapeutic strategies targeting NPC mobilization from germinal niches, whose effectiveness will depend on elimination of inflammation as well as on the long-term plasticity of the SVZ cells.

Supplementary material

Supplementary material is available at *Brain* online.

Acknowledgements

We thank John A. Alberta and Charles D. Stiles for providing the polyclonal antibodies specific for Olig1 (DF389) and Olig2 (DF308), Tatsunori Seki for providing the monoclonal antibody specific for PSA-NCAM (mAB12E3), Eugenio Montini for providing the CMV-GFP retrovirus (rkat 43.2), Giacomo Consalez for providing the *PDGF α* riboprobe, Vania Broccoli for providing the *Dlx2* riboprobe, and Angelo Corti for providing mouse TNF- α .

Funding

Italian Multiple Sclerosis Foundation (partial, 2004/R/15 to S.P. and 2005/R/15 to G.M.); the National Multiple Sclerosis Society (RG 3591-A-1 to G.M., partial RG-4000-A-1 to S.P. and RG 3945-A-10 to S.J.K.); the National Institutes of Health (AI 043496 and AI071448 to S.J.K.); the Italian Ministry of Research and University; Italian Ministry of Health, Banca Agricola Popolare di Ragusa and BMW Italy Group.

References

- Alvarez-Buylla A, Garcia-Verdugo JM. Neurogenesis in adult subventricular zone. *J Neurosci* 2002; 22: 629–34.
- Amadio S, Pluchino S, Brini E, Morana P, Guerriero R, Boneschi FM, et al. Motor evoked potentials in a mouse model of chronic multiple sclerosis. *Muscle Nerve* 2006; 33: 265–73.
- Bromberg JF, Horvath CM, Wen Z, Schreiber RD, Darnell JE Jr. Transcriptionally active Stat1 is required for the antiproliferative effects of both interferon alpha and interferon gamma. *Proc Natl Acad Sci USA* 1996; 93: 7673–8.
- Brown DA, Sawchenko PE. Time course and distribution of inflammatory and neurodegenerative events suggest structural bases for the pathogenesis of experimental autoimmune encephalomyelitis. *J Comp Neurol* 2007; 502: 236–60.
- Bull ND, Bartlett PF. The adult mouse hippocampal progenitor is neurogenic but not a stem cell. *J Neurosci* 2005; 25: 10815–21.
- Butovsky O, Ziv Y, Schwartz A, Landa G, Talpalar AE, Pluchino S, et al. Microglia activated by IL-4 or IFN-gamma differentially induce neurogenesis and oligodendrogenesis from adult stem/progenitor cells. *Mol Cell Neurosci* 2006; 31: 149–60.
- Calza L, Giardino L, Pozza M, Bettelli C, Micera A, Aloe L. Proliferation and phenotype regulation in the subventricular zone during experimental allergic encephalomyelitis: in vivo evidence of a role for nerve growth factor. *Proc Natl Acad Sci USA* 1998; 95: 3209–14.
- Carleton A, Petreanu LT, Lansford R, Alvarez-Buylla A, Lledo PM. Becoming a new neuron in the adult olfactory bulb. *Nat Neurosci* 2003; 6: 507–18.
- Chew LJ, King WC, Kennedy A, Gallo V. Interferon-gamma inhibits cell cycle exit in differentiating oligodendrocyte progenitor cells. *Glia* 2005; 52: 127–43.
- Doetsch F. The glial identity of neural stem cells. *Nat Neurosci* 2003; 6: 1127–34.
- Doetsch F, Caille I, Lim DA, Garcia-Verdugo JM, Alvarez-Buylla A. Subventricular zone astrocytes are neural stem cells in the adult mammalian brain. *Cell* 1999; 97: 703–16.
- Doetsch F, Garcia-Verdugo JM, Alvarez-Buylla A. Cellular composition and three-dimensional organization of the subventricular germinal zone in the adult mammalian brain. *J Neurosci* 1997; 17: 5046–61.
- Gartel AL, Serfas MS, Tyner AL. p21 – negative regulator of the cell cycle. *Proc Soc Exp Biol Med* 1996; 213: 138–49.
- Jackson EL, Garcia-Verdugo JM, Gil-Perotin S, Roy M, Quinones-Hinojosa A, Vandenberg S, et al. PDGFR alpha-positive B cells are neural stem cells in the adult SVZ that form glioma-like growths in response to increased PDGF signaling. *Neuron* 2006; 51: 187–99.
- Jin K, Wang X, Xie L, Mao XO, Zhu W, Wang Y, et al. Evidence for stroke-induced neurogenesis in the human brain. *Proc Natl Acad Sci USA* 2006; 103: 13198–202.
- Louis SA, Rietze RL, Deleyrolle L, Wagey RE, Thomas TE, Eaves AC, et al. Enumeration of neural stem and progenitor cells in the Neural Colony Forming Cell Assay. *Stem Cells* 2008; 26: 988–96.
- Mallamaci A, Muzio L, Chan CH, Parnavelas J, Boncinelli E. Area identity shifts in the early cerebral cortex of *Emx2*^{-/-} mutant mice. *Nat Neurosci* 2000; 3: 679–86.
- Martino G, Pluchino S. The therapeutic potential of neural stem cells. *Nat Rev Neurosci* 2006; 7: 395–406.
- Menn B, Garcia-Verdugo JM, Yaschine C, Gonzalez-Perez O, Rowitch D, Alvarez-Buylla A. Origin of oligodendrocytes in the subventricular zone of the adult brain. *J Neurosci* 2006; 26: 7907–18.
- Merkler D, Ernsting T, Kerschensteiner M, Bruck W, Stadelmann C. A new focal EAE model of cortical demyelination: multiple sclerosis-like lesions with rapid resolution of inflammation and extensive remyelination. *Brain* 2006; 129: 1972–83.
- Monje ML, Toda H, Palmer TD. Inflammatory blockade restores adult hippocampal neurogenesis. *Science* 2003; 302: 1760–5.
- Montini E, Cesana D, Schmidt M, Sanvito F, Ponzoni M, Bartholomae C, et al. Hematopoietic stem cell gene transfer in a tumor-prone mouse model uncovers low genotoxicity of lentiviral vector integration. *Nat Biotechnol* 2006; 24: 687–96.
- Morshead CM, Craig CG, van der Kooy D. In vivo clonal analyses reveal the properties of endogenous neural stem cell proliferation in the adult mammalian forebrain. *Development* 1998; 125: 2251–61.
- Morshead CM, Reynolds BA, Craig CG, McBurney MW, Staines WA, Morassutti D, et al. Neural stem cells in the adult mammalian forebrain: a relatively quiescent subpopulation of subependymal cells. *Neuron* 1994; 13: 1071–82.
- Morshead CM, van der Kooy D. Postmitotic death is the fate of constitutively proliferating cells in the subependymal layer of the adult mouse brain. *J Neurosci* 1992; 12: 249–56.
- Muzio L, Soria JM, Pannese M, Piccolo S, Mallamaci A. A mutually stimulating loop involving *emx2* and canonical wnt signalling specifically promotes expansion of occipital cortex and hippocampus. *Cereb Cortex* 2005; 15: 2021–8.

- Nait-Oumesmar B, Picard-Riera N, Kerninon C, Decker L, Seilhean D, Hoglinger GU, et al. Activation of the subventricular zone in multiple sclerosis: Evidence for early glial progenitors. *Proc Natl Acad Sci USA* 2007; 104: 4694–9.
- Picard-Riera N, Decker L, Delarasse C, Goude K, Nait-Oumesmar B, Liblau R, et al. Experimental autoimmune encephalomyelitis mobilizes neural progenitors from the subventricular zone to undergo oligodendrogenesis in adult mice. *Proc Natl Acad Sci USA* 2002; 99: 13211–6.
- Pinto L, Gotz M. Radial glial cell heterogeneity—the source of diverse progeny in the CNS. *Prog Neurobiol* 2007; 83: 2–23.
- Pluchino S, Quattrini A, Brambilla E, Gritti A, Salani G, Dina G, et al. Injection of adult neurospheres induces recovery in a chronic model of multiple sclerosis. *Nature* 2003; 422: 688–94.
- Politi LS, Bacigaluppi M, Brambilla E, Cadioli M, Falini A, Comi G, et al. Magnetic resonance-based tracking and quantification of intravenously injected neural stem cell accumulation in the brains of mice with experimental multiple sclerosis. *Stem Cells* 2007; 25: 2583–92.
- Raff MC, Abney ER, Cohen J, Lindsay R, Noble M. Two types of astrocytes in cultures of developing rat white matter: differences in morphology, surface gangliosides, and growth characteristics. *J Neurosci* 1983a; 3: 1289–1300.
- Raff MC, Miller RH, Noble M. Glial cell lineages in the rat optic nerve. *Cold Spring Harb Symp Quant Biol* 1983b; 48 (Pt 2): 569–72.
- Reynolds BA, Weiss S. Generation of neurons and astrocytes from isolated cells of the adult mammalian central nervous system. *Science* 1992; 255: 1707–10.
- Robinson DS, O'Garra A. Further checkpoints in Th1 development. *Immunity* 2002; 16: 755–8.
- Singec I, Knoth R, Meyer RP, Maciaczyk J, Volk B, Nikkhah G, et al. Defining the actual sensitivity and specificity of the neurosphere assay in stem cell biology. *Nat Methods* 2006; 3: 801–6.
- Takahashi T, Nowakowski RS, Caviness VS Jr. BUdR as an S-phase marker for quantitative studies of cytokinetic behaviour in the murine cerebral ventricular zone. *J Neurocytol* 1992; 21: 185–97.
- Zhang R, Zhang Z, Zhang C, Zhang L, Robin A, Wang Y, et al. Stroke transiently increases subventricular zone cell division from asymmetric to symmetric and increases neuronal differentiation in the adult rat. *J Neurosci* 2004; 24: 5810–5.
- Ziv Y, Ron N, Butovsky O, Landa G, Sudai E, Greenberg N, et al. Immune cells contribute to the maintenance of neurogenesis and spatial learning abilities in adulthood. *Nat Neurosci* 2006; 9: 268–75.